Neuron
Article

The Adaptive Trade-Off between Detection and Discrimination in Cortical Representations and Behavior

Douglas R. Ollerenshaw,[1,2,4] He J.V. Zheng,[1,4] Daniel C. Millard,[1] Qi Wang,[1,3] and Garrett B. Stanley[1,*]
[1]Coulter Department of Biomedical Engineering, Georgia Institute of Technology and Emory University, 313 Ferst Drive, Atlanta, GA 30332, USA
[2]Present address: Allen Institute for Brain Science, 551 North 34th Street #200, Seattle, WA 98103, USA
[3]Present address: Department of Biomedical Engineering, Columbia University, 351 Engineering Terrace, 1210 Amsterdam, Avenue, New York, NY 10027, USA
[4]These authors contributed equally to this work
*Correspondence: garrett.stanley@bme.gatech.edu
http://dx.doi.org/10.1016/j.neuron.2014.01.025

SUMMARY

It has long been posited that detectability of sensory inputs can be sacrificed in favor of improved discriminability and that sensory adaptation may mediate this trade-off. The extent to which this trade-off exists behaviorally and the complete picture of the underlying neural representations that likely subserve the phenomenon remain unclear. In the rodent vibrissa system, an ideal observer analysis of cortical activity measured using voltage-sensitive dye imaging in anesthetized animals was combined with behavioral detection and discrimination tasks, thalamic recordings from awake animals, and computational modeling to show that spatial discrimination performance was improved following adaptation, but at the expense of the ability to detect weak stimuli. Together, these results provide direct behavioral evidence for the trade-off between detectability and discriminability, that this trade-off can be modulated through bottom-up sensory adaptation, and that these effects correspond to important changes in thalamocortical coding properties.

INTRODUCTION

Adaptation has long been known to lead to changes in the nature of information flow in sensory pathways (Ahissar et al., 2000; Chung et al., 2002; Fairhall et al., 2001; Higley and Contreras, 2006; Khatri et al., 2009; Maravall et al., 2007). Although adaptation often leads to an overall decrease in neural activity sometimes interpreted as fatigue, a number of studies suggest more complex and important changes in coding properties in response to sensory adaptation that serve to improve information transmission in the face of complex inputs (Barlow, 1961; Clifford et al., 2007; Fairhall et al., 2001; Maravall et al., 2007; Moore, 2004; Moore et al., 1999; Sclar et al., 1989). More than half a century ago, von Békésy made the observation that the perceived size of a tactile stimulus decreased with increasing frequency of a repetitive sensory stimulus (von Békésy, 1957). More recent perceptual studies in humans have demonstrated that sensory adaptation can lead to improved discriminability of tactile stimuli applied to the skin (Goble and Hollins, 1993; Tannan et al., 2006; Vierck and Jones, 1970). Separately, a number of studies have investigated the spatial sharpening of cortical representations in somatosensory cortex in response to repetitive, ongoing sensory stimulation (Lee and Whitsel, 1992; Moore et al., 1999; Sheth et al., 1998; Simons et al., 2005; Tommerdahl et al., 2002), posited as a potential mechanism for enhanced spatial acuity (Lee and Whitsel, 1992; Moore et al., 1999; Vierck and Jones, 1970). However, the precise relationship between psychophysical findings and the underlying mechanisms responsible for these observations is unknown.

It has been asserted that detectability of sensory inputs can be sacrificed in favor of improved discriminability and that adaptation may regulate this trade-off (Crick, 1984; Moore, 2004; Moore et al., 1999; Sherman, 2001). In the visual pathway, it has been hypothesized that the thalamus serves to gate information flow, switching between dynamics that would facilitate detection of transient visual inputs at the level of cortex and those that would enable transmission of details of the visual input required for discrimination (Crick, 1984; Sherman, 2001). Although some neurophysiological evidence for this exists in the anesthetized animal (Lesica and Stanley, 2004; Lesica et al., 2006; Sherman, 2001), there is no direct behavioral support. In the specific context of the rodent vibrissa system, Moore (2004) hypothesized a trade-off between detection and discrimination mediated by the frequency content of tactile input. Relatedly, our recent work showed that adaptation serves to enhance discriminability of stimulus intensity at the expense of detectability from the perspective of an ideal observer of cortical activity and that adaptive modulation of thalamic firing properties may be a key player in this observation (Wang et al., 2010). In the context of spatial discriminability, reductions in overall cortical activation, coupled with spatial sharpening of the cortical response, suggest a similar sensory trade-off: detectability, or maximum sensitivity to unexpected tactile inputs, can theoretically be sacrificed

after adaptation to a stimulus in return for improved ability to discriminate or categorize the stimulus (Moore, 2004; Moore et al., 1999). To what extent these trade-offs exist behaviorally or electrophysiologically, however, is unknown.

Here, we utilized the rodent vibrissa pathway to directly test the adaptive trade-off between detection and discrimination in behavior to quantify the relevant information content in cortical representations that may underlie the behavior and to evaluate the adaptive effects on the thalamic inputs as a potential mechanism. Using voltage-sensitive dye (VSD) imaging of the cortex in anesthetized rats, we found that the reduction in the magnitude and sharpening of the cortical response resulted in enhanced spatial discriminability at the expense of detectability for an ideal observer of cortical activation. In a parallel set of behavioral experiments, rats were trained in vibrissa-based detection and spatial discrimination tasks, in which adaptation led to enhanced discrimination performance at the expense of stimulus detectability. Using a variably timed stimulus, we also determined the timescale of recovery from the effects of adaptation to be on the order of seconds. Recordings in the ventroposterior medial (VPm) nucleus of the thalamus of awake animals further revealed a reduction in spike count and timing precision with adaptation. Recovery of spike count and timing precision was found to be on a timescale that matched recovery in behavioral performance, and reductions in both quantities were predictive of a reduction in behavioral detection performance. Finally, the measured thalamic firing statistics were used to drive a model of the thalamocortical circuit, which demonstrated a sharpening effect with adaptation similar to that measured with VSD in the anesthetized animal. Together, these results provide direct behavioral and cortical evidence for the trade-off between detectability and discriminability, that this trade-off is modulated through bottom-up sensory adaptation, and that the underlying adaptive regulation of convergent thalamic input may play an important mechanistic role.

RESULTS

Adaptation Spatially Constrains the Cortical Response

We employed VSD imaging in the cortex of anesthetized rats to capture subthreshold activity of a large population of neurons in cortical layer 2/3 (Kleinfeld and Delaney, 1996; Petersen et al., 2003) as computer-controlled piezoelectric actuators deflected the vibrissae (Figure 1A). An anatomical barrel map was functionally registered to the images for illustration purposes (Wang et al., 2012). The cortical activation is reported as the percent change in fluorescence relative to the background level ($\%\Delta F/F_0$). The VSD signal initially appeared localized in the principal barrel at 10 ms after stimulus onset, quickly spread to neighboring barrels, peaked at approximately 20–25 ms, then gradually decayed back to baseline at approximately 100 ms, consistent with previous findings (Petersen et al., 2003; Wang et al., 2012). Subsequent analyses were based on the time-averaged response from the typical onset to peak time (10–25 ms).

Given the spatial spread of activation for a single whisker deflection, one immediate question is to what extent a single whisker stimulus activates adjacent barrels. An example of typical responses to separate deflections of two adjacent whiskers is shown in Figure 1B. Shown is the trial-averaged VSD response to whisker 1 (top) or whisker 2 (bottom) stimulation. Each of these responses was fit with a two-dimensional Gaussian function, the half-height contour of which was superimposed on the VSD image, and combined on the right. In the absence of any prior deflection of the vibrissae, the cortical response was recorded in what was referred to as the "nonadapted" state (Figure 1B). Following an ongoing, adapting stimulus, the cortical activation was recorded in response to the same test probe stimulus in the "adapted state" (Figure 1C). Note that the adapting stimulus in this case was a sequence of pulsatile (sawtooth) whisker deflections at a repetition rate of 10 Hz. Qualitatively, the nonadapted responses were spatially widespread (Figure 1B), with significant spatial overlap, whereas the adapted responses were spatially constrained and showed much less spatial overlap (Figure 1C; Figure S1 available online).

Adaptation Degrades Stimulus Detectability for an Ideal Observer

We measured the detectability of a stimulus against prestimulus noise on a single trial basis in the nonadapted and adapted states using optimal detection theory (Duda et al., 2001; Macmillan and Creelman, 2005). Each single-trial cortical response was represented as a decision variable (DV), which was used by the ideal observer to classify each trial as signal or noise. This was done by averaging the measured neural activity within an approximately barrel-sized region of interest (ROI) 10–25 ms after stimulus onset. Note that the results were not dependent on absolute ROI size, as long as it remained within the range of an individual cortical column (300–500 μm in diameter). For each case, the DVs over all 50 trials were binned and a Gaussian probability function was fit. Figure 2A shows a typical example of the noise (shown in black) and signal distributions in the nonadapted (gray) and adapted (orange) states (same ROI for all). Corresponding examples of trial-averaged VSD responses are shown for each of the three cases with the decision region overlaid in black. The adapted distribution lies closer to the noise than does the nonadapted, implying a reduction in detectability with adaptation. We measured detectability using a standard detection theory variable, d′, which quantifies the separability between two distributions. There was a significant decrease in detection performance (d′ between signal and noise) after adaptation (Figure 2B; nonadapted d′: 1.24 ± 0.076; adapted d′: 1.05 ± 0.078; $p < 0.005$, $n = 18$, paired t test). Results were very similar using a related measure derived from the receiver-operating characteristic (ROC) curve (Figures S2O and S2P).

Adaptation Enhances Stimulus Discriminability for an Ideal Observer

The ideal-observer analysis was extended to measure changes in spatial discriminability resulting from deflections of adjacent vibrissae in the nonadapted and adapted states. Based on the cortical response to a single whisker deflection, the observer was tasked with identifying which of two possible whiskers caused it. The ROIs for the two whiskers were defined as described above and were applied to all single trials. After a deflection of whisker 1, we measured the response in the corresponding ROI ($R_1|W_1$) as well as the response in the adjacent ROI

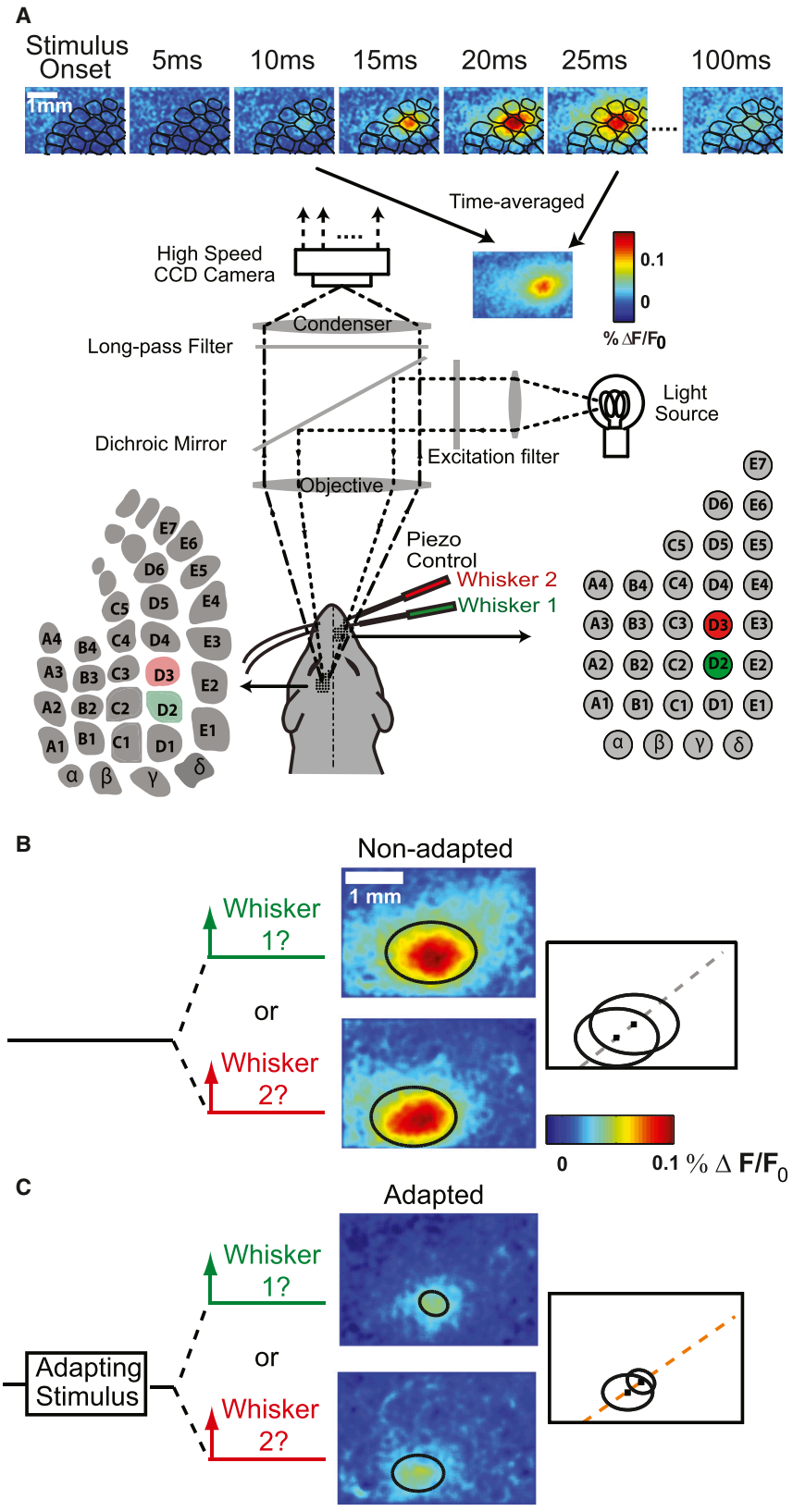

Figure 1. In Vivo VSD Imaging of the Rat Barrel Cortex

(A) A piezoelectric actuator delivered a probe deflection to either of two adjacent whiskers while a camera system simultaneously collected fluorescence signal from layer 2/3 of an anesthetized rat. The top panel shows an example response to a single whisker deflection (850°/s, rostral-caudal) averaged over 50 trials. Overlaid on the VSD images is an outline of barrels functionally registered using the responses to different whisker deflections.

(B) The cortical responses to a single-whisker stimulation in the absence of a preceding 10 Hz adapting stimulus. Whisker 1 (W1) and whisker 2 (W2) were adjacent to each other on the snout and stimulated separately. Images were averaged over 50 trials. The black ellipses on the images were half-height contours of the two-dimensional Gaussian fits to the images. On the right is the superposition of the Gaussian contours.

(C) In contrast, the same stimulus following a 10 Hz adapting stimulus evoked a cortical response that was significantly reduced in magnitude and in area. See also Figure S1.

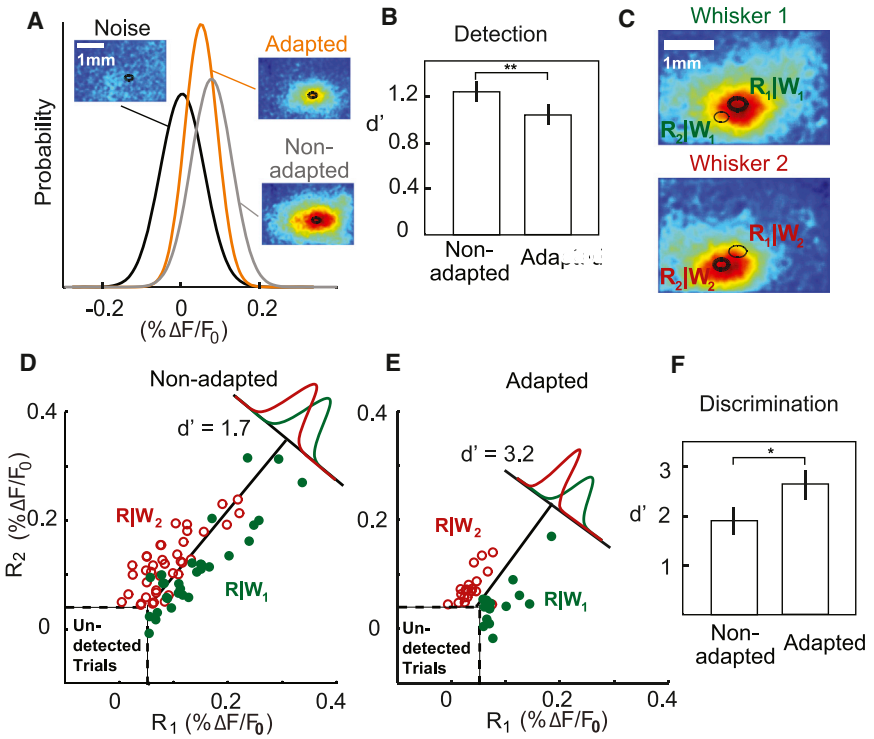

Figure 2. Ideal Observer Analysis: Adaptation Enhances Discrimination at the Expense of Detection

(A) A region of interest (ROI) approximately the size of a cortical column (300–500 μm in diameter) was defined as the 98% height contour of the two-dimensional Gaussian fit to the trial-averaged nonadapted response. The insets show the corresponding trial-averaged images for each case (noise, nonadapted, and adapted), with the ROI outlined in black (same in all cases). The average fluorescence within the ROI was extracted from each single trial as a decision variable (DV).

(B) The d′ value, a measure of the separation of the signal and noise distributions, decreased following adaptation ($p < 0.005$, $n = 18$, paired t test).

(C) The same method described in the detection analysis was used to derive the ROI for each of the two whisker stimulations (shown in bold ellipse). Both ROIs were applied to all single trials. Two responses were calculated for each single trial: the average fluorescence within the principal barrel area (bold ellipse) and that within the adjacent barrel area (thin ellipse).

(D) Responses above the detection threshold in the nonadapted case were grouped by whisker stimulation and separated using linear discriminant analysis (LDA). The decision variable was defined as the projection of the response onto the axis orthogonal to the LDA line. The d′ separation measure was then calculated for the two probability distributions of the decision variables. The d′ in this example was 1.7.

(E) Same analysis as in (D) for the adapted case. The d′ in this example was 3.2.

(F) Discrimination performance (d′ of DV probability distributions) of the ideal observer significantly improved following adaptation ($p < 0.05$, $n = 9$, paired t test).

All error bars represent ±1 SEM. See also Figure S2.

($R_2|W_1$). Figure 2C shows the response to each whisker deflection, with the two ROIs outlined in black. For a given whisker deflection, the corresponding ROI is shown in bold.

Figure 2D shows an example of all single-trial variables for a single data set. Each point represents a single trial, with responses from deflections of whisker 1 shown in green (closed circles) and those from deflections of whisker 2 shown in red (open circles). Trials were excluded from analysis when the response fell below the "detection threshold," which corresponded to a detection false alarm rate of 10%, based on the false alarm rate from related behavioral studies (Ollerenshaw et al., 2012; Stüttgen and Schwarz, 2008). The extent to which these two clusters can be discriminated determines how well an observer could correctly identify which whisker led to a particular cortical response. Linear discriminant analysis (LDA) was used to determine the line that maximally separated the two clusters, shown as the solid black line in Figure 2D. The raw variables were projected onto the line orthogonal to the LDA line, and the separability of the two probability distributions, measured using the standard detection theory variable d′, was used as the discrimination metric.

Figure 2E shows the adapted case, where the two variable clusters became more separated, resulting in a larger separation of the probability distributions. Due to the simultaneous reduction in signal amplitude, a higher percentage of trials fell below the detection threshold and were subsequently eliminated from the analysis. Discriminability was significantly improved following adaptation (Figure 2F, nonadapted d′: 1.9 ± 0.24; adapted d′: 2.6 ± 0.26; $p < 0.05$, $n = 9$, paired t test). Figures S2A–S2N show single-trial examples, and the trial averages for both the correctly and incorrectly classified whisker-deflection responses are shown in Figures 2D and 2E. Similar results emerged from a likelihood ratio test, and results were relatively insensitive to chosen parameters (Supplemental Experimental Procedures; Figure S2Q).

The Behavioral Trade-Off between Detection and Discrimination with Adaptation

To directly test the perceptual effects of sensory adaptation, both a detection and spatial discrimination task were carried out using a separate set of head-fixed rats. The detection task was modeled closely off of detection tasks published previously by our lab and others (Ollerenshaw et al., 2012; Stüttgen and Schwarz, 2008), with the exception that the stimulus to which animals were trained to respond was preceded by a 12 Hz sinusoidal adapting stimulus on a subset of trials (Figure 3A). Each trial in the task was initiated by a 3 s tone, during which an adapting stimulus was presented randomly on half of the trials. A variable velocity stimulus was presented on a uniformly varying time interval between 0.5 and 2.5 s after the end of the tone, and

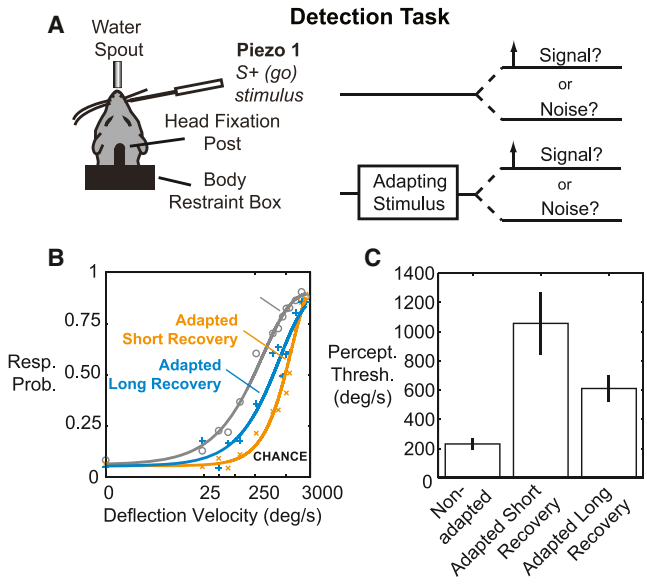

Figure 3. Behavioral Detection Thresholds Are Increased with Adaptation

(A) Detection task. A piezoelectric actuator was placed on a single whisker, and a variable velocity probe stimulus was presented at a randomized time. The probe was preceded by an adapting stimulus on 50% of trials.

(B) Combined psychometric curve for all animals for the nonadapted (gray) and the adapted short recovery (orange) and long recovery (blue) cases. Error bars are omitted for clarity. The black dashed line indicates the chance performance level.

(C) Quantification of perceptual thresholds. Each bar represents the perceptual threshold, measured as the 50% point of the sigmoidal fit (nonadapted to adapted short recovery: $p < 0.05$; nonadapted to adapted long recovery: $p < 0.05$; paired t test, $n = 4$). Error bars represent ±1 SEM.

See also Figure S3.

animals had a 1 s window following the stimulus in which to emit a lick to receive a water reward (Figure S3A).

Adaptation Degrades Stimulus Detectability for Awake, Behaving Animals

Figure 3B shows the psychometric curves that resulted from the behavioral detection experiments for all animals (see Figure S3B for sample raw data). The black dashed line labeled as "chance" indicates the response probability on catch trials, in which a deflection of a second piezoelectric actuator was substituted for the actuator attached to a whisker. The response probability on catch trials was 8.7% on nonadapted trials and 8.6% on adapted trials, which is consistent with the behavioral false alarm rate from similar studies (Ollerenshaw et al., 2012; Stüttgen and Schwarz, 2008) and also demonstrates that adaptation did not lead to a change in response criterion for the animals.

The orange curve in Figure 3B shows the combined psychometric curve in response to stimuli falling in the short recovery period (0.5–1.5 s following adaptation). The curve is shifted to the right relative to the nonadapted (gray) curve, indicating that a much stronger stimulus must be delivered to achieve the same response probability. Importantly, the response probability for the strongest stimulus approached that seen in the nonadapted case, indicating that the change in performance is not due simply to changes in motivational level, or confusion on the part of the animals. The blue curve shows the psychometric function for stimuli occurring in the long recovery period (1.5–2.5 s following adaptation), indicating a return to baseline detection performance.

The observed decrease in detectability was quantified by measuring the change in the perceptual threshold, defined as the 50% point on the psychometric curve. Figure 3C shows the average threshold (232 ± 35 /s, nonadapted), which is very similar to that seen in a similar single-whisker detection task (Stüttgen and Schwarz, 2008). The average threshold increased to 1,057 ± 204 /s in the adapted short recovery state and then decreased to 611 ± 81 /s in the adapted long recovery state. Thus, detectability was reduced following adaptation to a sensory stimulus, with a 4-fold increase in stimulus velocity required to achieve the same threshold performance level ($p < 0.05$, $n = 4$, paired t test). Performance began to recover with timescales on the order of a few seconds, though detection thresholds remained significantly above those in the nonadapted state ($p < 0.05$, $n = 4$, paired t test). Reaction times were also observed to increase following adaption (Figure S3).

Adaptation Improves Spatial Discriminability in Awake, Behaving Animals

Animals were then trained on a two-whisker go/no-go spatial discrimination task (Figure 4A). The S+ or "go" whisker remained the same as in the detection task. However, a second piezoelectric actuator was attached to a second nearby whisker, which was deemed the S or "no-go" whisker. The task proceeded as it had during the detection task, with the exception that on a given trial, the stimulus was randomly chosen as either the S+ or S whisker with equal probability. To avoid cueing the animal as to which whisker would be stimulated, both whiskers were deflected together during the adaptation phase of the trial. The velocity of the probe stimulus remained fixed at 1,500 /s. Animals were rewarded for responding to the S+ stimulus as before but were penalized with a 5–10 s timeout paired with the house lights when they responded to the S stimulus.

Figure 4B shows the summary of response probabilities for all trials averaged across all animals, with corresponding raw data shown in Figures S4C and S4D. Hit and false alarm rates are shown in green and red, respectively. The three possible states of adaptation are presented from top to bottom. As expected based on the detection results, the overall hit and false alarm rates decreased from the nonadapted to adapted short recovery state (shown schematically in Figures S4A and S4B) and then increased somewhat with a longer period of recovery. However, it is difficult to determine from these values alone whether any change in discrimination performance exists across the states. Figure 4C shows that when the ratio of hit rate to false alarm rate was calculated, there was a significant increase in discrimination performance from the nonadapted state to the adapted short recovery state, with the ratio increasing from 1.44 ± 0.14 to 2.11 ± 0.19 ($p < 0.005$, $n = 5$, paired t test). With a longer recovery period, the discrimination performance decreased (hit to false alarm ratio of 1.72 ± 0.17), though it remained significantly above the nonadapted value ($p < 0.05$, $n = 5$, paired t test), indicating that recovery was not complete by 2.5 s after the end of

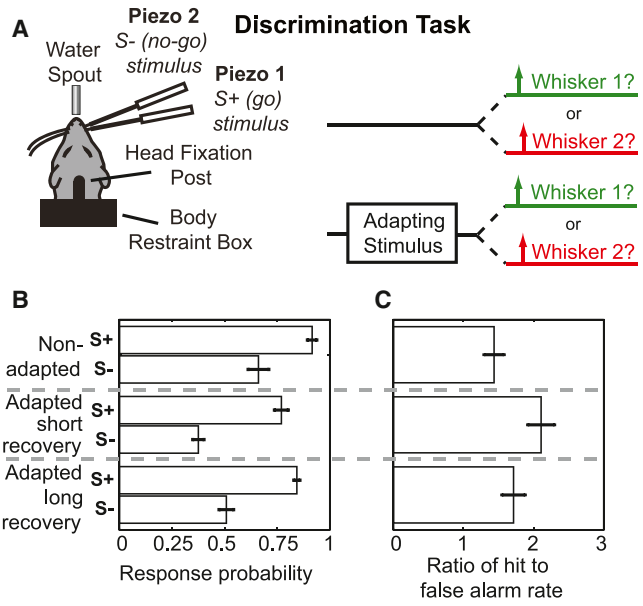

Figure 4. The Spatial Discrimination Performance of the Animals Is Improved with Adaptation

(A) Discrimination task. A second piezoelectric actuator was introduced on a nearby whisker. The task proceeded as in the detection task, with the exception that on a given trial either the S+ (go whisker) or the S (no-go) whisker was deflected with equal probability using a fixed suprathreshold velocity. Animals were rewarded as before for responses to the S+ stimulus but were penalized with a timeout for responses to deflections of the S whisker.

(B) Raw response probabilities. Response probabilities to S+ and S stimuli are shown in green and red. From top to bottom, each pair of bars represents the nonadapted state, the adapted short recovery state, and the adapted long recovery state.

(C) Discriminability quantified as the ratio of the hit rate to the false alarm rate. Discriminability is measured using the data in (B) for the nonadapted (gray), adapted short recovery (orange), and adapted long recovery (blue) states (nonadapted to adapted short recovery: $p < 0.005$; nonadapted to adapted long recovery: $p < 0.05$; paired t test, $n = 5$). All error bars represent ±1 SEM. See also Figure S4.

adaptation. Two additional measures of discriminability, the detection corrected d′ (Figure S4E) and the discrimination index (Figure S4F), both showed similar trends. Reaction times in the discrimination task are summarized in Figure S4G. Reaction times were longer than in the detection task, but animals demonstrated a similar increase following adaptation.

Adaptation of the Thalamocortical Circuit of Awake, Behaving Animals

We have previously demonstrated that adaptive shifts in cortical feature selectivity are strongly correlated with changes in thalamic firing and synchronization with adaptation (Wang et al., 2010). To uncover potential mechanisms underlying our observations here and to provide a link between the cortical activation and behavior, neural recordings were obtained from the ventroposterior medial (VPm) nucleus of the thalamus in three awake rats. Two of those animals were also trained to perform the detection with adaptation task described above.

The effect of adaptation to a pulsatile (sawtooth) stimulus at a base rate of 10 Hz can clearly be seen in Figure 5A, showing the average peristimulus time histogram (PSTH) of multiunit activity across all sessions of all three animals (see Figures S5A–S5F for sample raw data). Figure 5B shows the mean normalized spike count across all sessions, which displayed a sharp decrease in firing rate from the first to the second pulse in the adapting train, recovered slightly, then approached a steady-state level of adaptation of 79.2% of the nonadapted firing rate.

Here, we used timing precision of the multiunit recording as a proxy for population synchrony across multiple single units within a barreloid (Butts et al., 2007; Desbordes et al., 2008). A quantitative measure of timing precision is the "temporal contrast," or TC40 metric (Pinto et al., 2000). TC40 is defined as the number of spikes representing 40% of the total response magnitude in a 30 ms poststimulus window, divided by the time required to generate the first 40% of the total response magnitude. Figure 5C shows that timing precision decreased by approximately 33%, from 0.217 spikes/ms (nonadapted) to 0.145 spikes/ms (adapted), with the qualitative effects shown in the inset, very similar to the percentage reduction in synchrony measured in the anesthetized animal (Wang et al., 2010). See Figures S5G–S5I for additional measures.

Thalamic Adaptation Recovers on a Similar Timescale as Behavioral Detection Performance

The number of elicited spikes and timing precision in the nonadapted and adapted states are shown in Figures 6A and 6C, respectively. In both cases, the short recovery (shown as orange Xs) and long recovery (shown as blue Os) values were plotted against the nonadapted values. Both the spike count and the timing precision of thalamic firing in response to a probe decreased from their nonadapted levels. However, in general, the short recovery values lie further below the unity line (orange Xs tend to lie below the blue Os), indicating the effects of adaptation are more profound with short periods of recovery. Figure 6B shows that the firing rate was reduced to 78% ± 2.7% of the nonadapted value for short recovery periods ($p < 0.005$, $n = 43$, paired t test), then began to recover to 84% ± 2.6% of the nonadapted value ($p < 0.005$, $n = 43$, paired t test) with additional time for recovery. Similarly, timing precision as measured using TC40 was reduced to 81% ± 3.0% of the nonadapted value with a short period of recovery ($p < 0.005$, $n = 43$, paired t test) and increased to 87% ± 3.0% of its nonadapted value ($p < 0.05$, $n = 43$, paired t test) with additional recovery time (Figure 6D). When trials were separated based on the behavioral outcome (Figures S5J and S5K) in the detection task (two of the three implanted animals were trained on the task), both the spike count and the timing precision, as measured using TC40, were lower on miss trials versus hit trials ($p < 0.05$ for both quantities, paired t test, $n = 53$). Taken together, the spiking activity measured in the VPm thalamus of the awake animal strongly mirrored the behavioral findings obtained throughout the study.

A Model of the Thalamocortical Circuit Predicts Cortical Sharpening with Adaptation

To link the measured effects of adaptation in the thalamus with the improvements in spatial discriminability and the

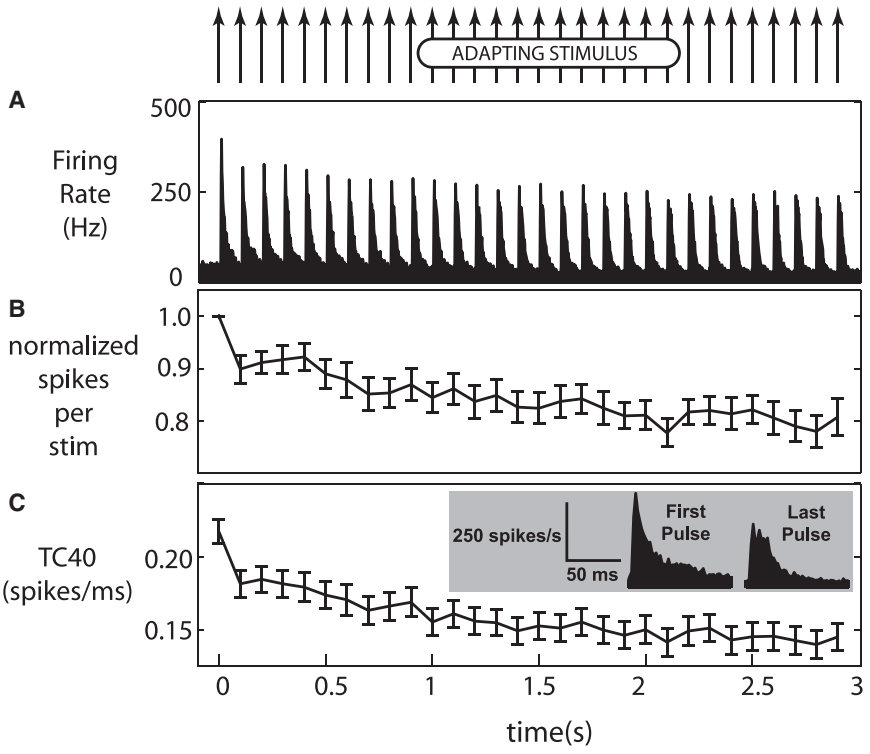

Figure 5. Adaptation of Thalamic VPm Cells in the Awake Animal

(A) The combined PSTH for all animals and recording sessions.

(B) The number of spikes per stimulus for each pulse in the 3 s, 10 Hz train of adapting stimuli, normalized to the spike count in response to the first pulse. After adaptation, the firing rate was 79.2% of its nonadapted value.

(C) Timing precision, as measured using TC40, decreased from 0.217 ± 0.008 spikes/ms in the nonadapted state to 0.145 ± 0.008 spikes/ms after adaptation. The inset shows the first and last PSTH combined across all animals and recording sessions. All error bars represent ±1 SEM (all values $p < 0.005$, $n = 56$, two sided t test comparing response to first pulse with response to the final three pulses combined).

See also Figure S5.

corresponding changes in cortical processing, a model (Figure 7A) was used to simulate the cortical response to thalamic inputs in both the nonadapted and adapted states. The model consisted of excitatory thalamic input to cortical excitatory (regular-spiking units) and inhibitory (fast-spiking units) neurons, with intracortical connectivity across the excitatory and inhibitory subpopulations. The inputs to the model were based on the thalamic data recorded from the awake animal that was reported above. Note that VSD imaging captures subthreshold activity in layer 2/3 of cortex, whereas the model here captured the firing rates in cortical layer 4. The early-onset frames of cortical activation as measured by layer 2/3 VSD imaging have been shown to be reflective of the suprathreshold activation of layer 4 cortical neurons (Petersen et al., 2003).

The cortical outputs of the model are shown in Figure 7B, in which a much sharper response is qualitatively apparent after sensory adaptation. To quantify the changes in the sharpness of the cortical response, the difference in normalized activation between the principal and adjacent barrels was calculated. The difference in normalized activation levels can range from 0 (no difference between activation in the principal and adjacent barrels) to 1 (activity only in the principal barrel). The model demonstrated an increase in this quantity from 0.27 ± 0.14 in the nonadapted state to 0.57 ± 0.24 in the adapted state (Figure 7C). It was also possible to measure the individual effects of changing just the firing rate while leaving the timing synchrony fixed. This led to a much smaller normalized difference in activation levels of 0.39 ± 0.21 ("synchrony controlled," Figure 7C; black line, Figure 7B). From the perspective of an ideal observer, these differences correspond to discriminability, measured as d′, of 2.76, 2.58, and 3.26 for the nonadapted, synchrony-controlled, and adapted states, respectively. This represents a predicted 18% increase in discriminability with adaptation, with the synchrony-controlled condition actually representing a slight (6%) decrease. Although these d′ values represent better discriminability than was obtained in the ideal observer analysis presented above, no attempt was made to add noise to the model that would degrade overall discriminability but preserve the adaptation effects. Taken together, the results here suggest that the adapting stimulus paradigm utilized in the behavior had a significant effect on the thalamic firing properties in the awake animal, that thalamic firing correlated with detection performance, and that the adaptive modulations in both thalamic firing rate and synchrony likely play a role in the sharpening of the spatial activation in cortex that we showed to result in an enhanced discriminability at the expense of detectability.

DISCUSSION

In the presence of persistent stimulation, sensory systems have long been shown to exhibit various forms of rapid and reversible adaptation (Ahissar et al., 2000; Barlow, 1961; Chung et al., 2002; Fairhall et al., 2001; Higley and Contreras, 2006). It has been posited that these forms of adaptation do not represent deleterious reductions in firing, but instead represent fundamental changes in coding properties that likely possess ethological relevance. Specifically, in the vibrissa system, the animal's own whisking motion has been proposed to lead to a state similar to that achieved through adaptation to passively applied stimuli, switching the system from a state in which it is more sensitive to inputs to one in which it is more selective (Moore, 2004; Moore et al., 1999). Under this scenario, inputs arriving when the pathway is in the nonadapted state are more likely to generate a large cortical response, alerting an otherwise quiescent or inattentive animal to the presence of an unexpected stimulus (Chung et al., 2002; Diamond and Arabzadeh, 2013; Fanselow and

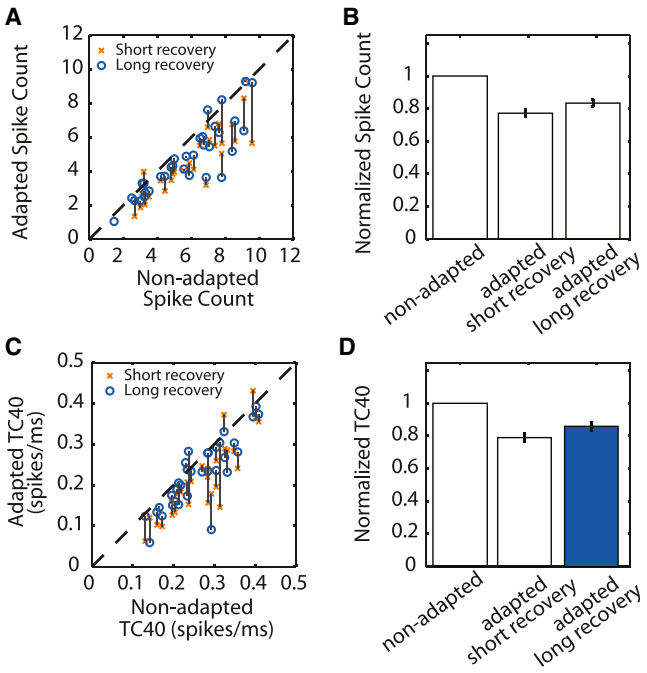

Figure 6. Firing Rate and Timing Precision in Response to the Probe Stimulus

(A) Scatterplot of spikes in a 30 ms window following the probe stimulus. On a given session, both the mean spike count in response to short recovery stimuli (those falling in the 0.5–1.5 s postadaptation window, shown as orange Xs) and long recovery stimuli (those falling in the 1.5–2.5 s post adaptation window, shown as blue Os) are plotted against the mean number of spikes elicited by nonadapted probe stimuli. Gray lines connect data points from a given session.

(B) Same data as (A), but each data point is normalized against the nonadapted value.

(C) Scatterplot of firing precision measured as TC40. Same conventions as (A).

(D) Same data as (C), but each data point is normalized against the nonadapted value. All error bars represent ±1 SEM.

Nicolelis, 1999; Khatri et al., 2009; Sherman, 2001), presumably at the expense of specificity. However, with active exploration of an object, the system is placed into an adapted state, subsequently reducing the magnitude of the cortical response but improving the ability of the system to discern the finer features of sensory stimuli (Fanselow et al., 2001; Kohn and Whitsel, 2002; Maravall et al., 2007; Moore, 2004). Studies with freely behaving rodents have demonstrated that the cortical response to peripheral inputs is reduced when the animal is whisking (Castro-Alamancos, 2004; Crochet and Petersen, 2006; Fanselow and Nicolelis, 1999; Ferezou et al., 2007; Hentschke et al., 2006; Poulet et al., 2012), and exploratory whisking in air drives activity along the pathway (Leiser and Moxon, 2007), potentially implying that the animal's own self-motion serves to place it into an adapted state similar to that described here. Indeed, detectability is significantly improved in the absence of whisking (Ollerenshaw et al., 2012), potentially part of an active strategy by the animal to facilitate information flow in this very specific context. Although the frequencies of the adapting stimuli used in the present study were chosen to fall within the natural 5–15 Hz whisking range (Brecht et al., 1997; Carvell and Simons, 1990), a more complete characterization of the effects of adaptation across a broader range of frequencies would be important in understanding how natural behaviors modulate the observed detectability/discriminability trade-off.

Combined, our behavioral results and the corresponding thalamic recordings unambiguously demonstrate the existence of sensory adaptation in the thalamocortical circuit and that this adaptation leads to measureable perceptual changes. Relevant to the findings here, a previous study suggested that sensory adaptation at the level of the thalamocortical circuit was largely absent in rodents during active behavioral states (Castro-Alamancos 2004). This was attributed to the fact that when animals were in novel environments and engaged in exploratory behavior, the cortical response to the first stimulus in a train of adapting stimuli was already reduced, limiting the ability to further reduce the response with adaptation. It was asserted that, in effect, the cortex was already in an adapted state during active states. However, it should be noted that this lack of adaptation in the awake state was limited to periods in which the animal was involved in exploratory behavior or engaged in a novel task. The adaptation effect returned after the animals became familiar with a trained task. Given that the animals in our behavioral experiments were exposed to the tasks over the course of many weeks, they were likely operating in this regime of familiarity, and thus would be expected to show the effects of adaptation. This point strongly argues for the existence of a wide range of behavioral states in the awake animal, each potentially with goal-specific neural processing characteristics (Fanselow and Nicolelis, 1999; Ferezou et al., 2007), and the characteristics we observed in the anesthetized state may be representative of a subset of the available processing states in the awake animal. In any case, our results demonstrate that clear signatures of adaptation are present in the thalamus of the awake animal in the context of precisely controlled sensory inputs in a behavioral task and that even relatively moderate adaptive changes in thalamic firing rate and timing precision can have fairly dramatic effects on the downstream cortical representation. Further, the evidence presented here strongly suggests that the improved discriminability with adaptation results from a sharpening of the spatial response at the level of S1. Intrinsic optical imaging results in the anesthetized monkey have pointed to such a sharpening effect with adaptation (Simons et al., 2005; Tommerdahl et al., 2002). In previous studies in the vibrissa pathway, some evidence for spatial sharpening has been demonstrated in single-unit recordings (Brumberg et al., 1996), local field potentials and intrinsic optical imaging (Sheth et al., 1998), and VSD imaging (Kleinfeld and Delaney, 1996), leading to speculation that this could enhance discriminability (Moore, 2004; Moore et al., 1999).

A wide range of studies characterizing cortical representations in the face of persistent or adapting stimuli (Lee and Whitsel, 1992; Sheth et al., 1998; Simons et al., 2005) have made qualitative inferences regarding the relationship between the observed spatial sharpening and the improved acuity in psychophysical studies (Tannan et al., 2006; Vierck and Jones, 1970). It is important to note, however, that a sharpened cortical response alone is not sufficient to improve discriminability and that in many cases sharpened representations can lead to a reduction in

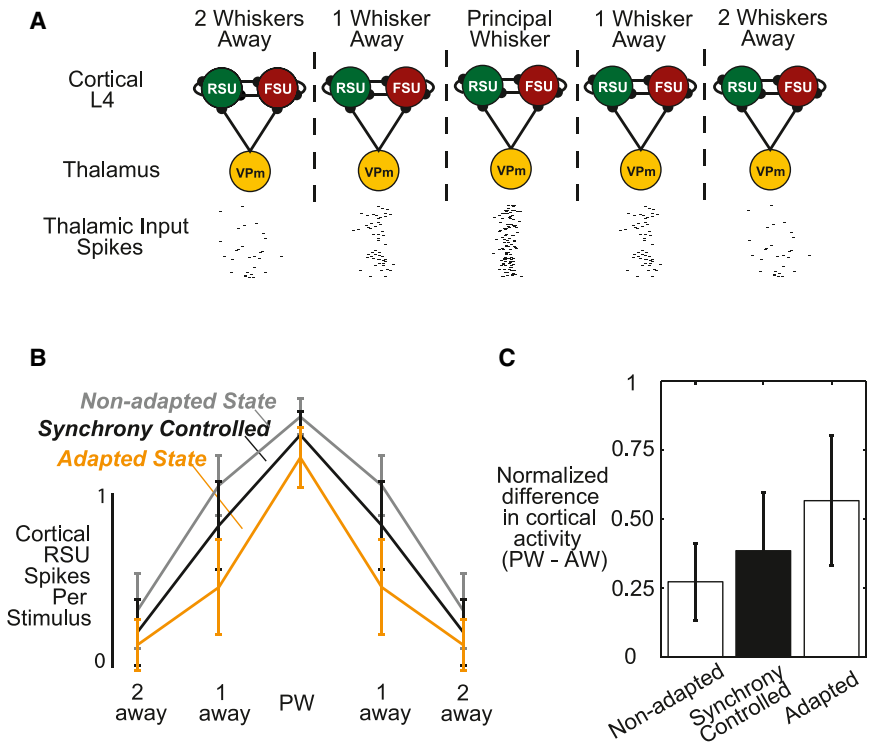

Figure 7. Simulated Cortical Response from Experimentally Measured Changes in Thalamic Firing in the Awake Animal

(A) A schematic of the model configuration. Each barreloid-to-barrel connection is treated as an isolated circuit. Each thalamic barreloid in VPm nucleus of the thalamus contains only excitatory relay cells. The input neurons in layer 4 of the cortex consist of both excitatory regular-spiking units (RSUs) and inhibitory fast-spiking units (FSUs). These cells receive both thalamocortical and intracortical inputs. Sample thalamic input spike trains are shown below each column, demonstrating the reduction in precision and spike count with distance from the principal whisker (PW) that is built into the model.

(B) The output of the model, which is the number of spikes generated by the regular spiking units in each barrel, in response to a deflection of the PW. The black line represents trials in which only the spike count was allowed to adapt but the timing precision was held constant.

(C) The sharpness of the cortical response, here measured as the difference in normalized activity in the principal and adjacent whiskers. The response was strongly sharpened with adaptation. However, when allowing only the firing rate to change with adaptation but holding timing synchrony constant before and after adaptation (labeled as synchrony controlled), the sharpening effect is less pronounced. The increased cortical sharpness with adaptation predicts improved discriminability. All error bars represent ±1 SD.

information transmission (Pouget et al., 1999). Here, we considered both the mean, trial-averaged cortical responses, which provide the qualitative "sharpening" of the cortical response we observe with adaptation, and the trial-by-trial cortical activation that the animal would have access to in a behavioral context. From the classical signal-detection perspective, the key measure of being able to discriminate between sensory inputs lies in the separability of the probability distributions of the assumed response variable. A major contribution here, which goes above and beyond the previous studies where sharpened cortical responses have been demonstrated, is that the quantitative trial-by-trial analysis demonstrated a measureable enhancement in discriminability, a result that was not preordained by the sharpened cortical representations alone. This is even more the case given the fact that the adaptation unambiguously reduces neural activity in cortex even at the center of cortical activation, which could produce a wide range of perceptual effects.

As with linking any behavioral percept to the underlying neural activity, it cannot be directly asserted that the percepts utilized by the animal to perform the detection and discrimination tasks in this study exist in S1. However, the ideal observer analysis shows us that the necessary information is present at this level of processing and that the adaptive modulation of the detectability/discriminability trade-off is also reflected at this stage. The neural activity in the primary sensory cortex has long been considered the fundamental neural basis for downstream sensory percepts and behavior. However, there are some contradictory experimental studies on this point, with some demonstrating a complete abolishment of abilities to perform whisker-related tasks with the inactivation of S1 (O'Connor et al., 2010), others demonstrating only a severe degradation of detection abilities (Hutson and Masterton, 1986; LaMotte and Mountcastle, 1979), and some studies showing that microstimulation of S1 directly influences an animal's stimulus detection and discrimination performance (Houweling and Brecht, 2008; Huber et al., 2008; Romo et al., 2000). Taken together, we can, at minimum, conclude that S1 is a major role-player in simple behaviors such as detection.

Despite the fairly widely observed phenomenon of spatial sharpening of cortical representations, the underlying mechanism has not been explored extensively. One possibility long postulated involves the dynamic engagement of inhibitory mechanisms at the level of cortex or more peripherally, shifting the E/I balance (von Békésy, 1957; Kyriazi and Simons, 1993; Mountcastle and Darian-Smith, 1968; Simons and Carvell, 1989; Simons et al., 1992). Using microelectrode recordings of single units in S1, Brumberg et al. (1996) demonstrated that when a whisker was continuously stimulated with white noise, the deflection of an adjacent whisker led to a more constrained cortical response than when the whisker was deflected alone, a result that could be attributed to thalamic decorrelation, as supported by the thalamic recordings and corresponding cortical network simulations here. The complementary results in both the anesthetized and awake animals demonstrated here would seem to indicate that the improved discriminability with adaptation cannot be fully explained by top-down mechanisms (Gilbert and Li, 2013), which are of course absent in the anesthetized animal. Sensory adaptation has been shown to

lead to a decrease in firing synchrony of thalamic neurons (Temereanca et al., 2008), a phenomenon that has been shown to lead to decreased stimulus detectability and improved velocity discriminability at the cortex (Wang et al., 2010) due to the extreme sensitivity of layer 4 cortical neurons to the timing of thalamic inputs (Alonso et al., 1996; Bruno, 2011; Roy and Alloway, 2001; Stanley et al., 2012; Usrey et al., 2000) and its importance in determining cortical feature selectivity (Stanley, 2013; Stanley et al., 2012). As shown through our chronic recordings of VPm activity in the awake animal and the corresponding thalamocortical network model simulations, the reduced spread of cortical activity seen in the VSD imaging experiments could reflect a less synchronous drive from the thalamus. This could result from a reduced activation of nonaligned regions of the cortex through the interactions between network connectivity and cortical sensitivity to the synchrony of thalamic inputs (Bruno, 2011).

The focus here has been on the relationship between detection of transient tactile inputs and corresponding spatial discriminability, but it is possible that this concept extends to other pathways and ethologically relevant contexts. In the visual pathway, for example, there is a substantial body of work related to modulation of states that facilitate detection of transient inputs, such as an object moving into the visual field, and states that facilitate the transmission of information about the fine details of the scene (Crick, 1984; Sherman, 2001) and about how this may relate to the natural visual environment (Lesica and Stanley, 2004), but this has not been explicitly shown to be behaviorally relevant. In the somatosensory pathway, the discriminability described here may extend to textural properties of object surfaces, suggested by corresponding psychophysical studies in humans (Tannan et al., 2006; Vierck and Jones, 1970; Goble and Hollins, 1993), which would be captured in patterns of transient whisker motion in the vibrissa system. How adaptation may modulate the relationship between object contact (detection) and transmitting the details of textural properties of object surfaces is unknown. Across sensory modalities and across features within a sensory modality, the adaptive changes we describe here could act to improve the ability of the system to discriminate between stimuli, consistent with the long-held theoretical notion that adaptation acts to enhance information transmission in sensory pathways (Barlow, 1961; Moore, 2004; Moore et al., 1999). To be more precise, however, we assert that increasing adaptation enhances information transmission about the details of the sensory input, whereas decreasing adaptation serves to enhance information about the presence of the sensory input, perhaps acting on a continuum of processing states. Concerning information transmission, it is thus important to precisely define the nature of the information in question (Stanley, 2013). Increasing or decreasing the degree of sensory adaptation shifts the system from transmitting information about one aspect of the environment to another, potentially a hallmark of sensory processing in the natural sensory world (Lesica and Stanley, 2004).

EXPERIMENTAL PROCEDURES

All procedures were approved by the Institutional Animal Care and Use Committee at the Georgia Institute of Technology and are in agreement with guidelines established by the National Institutes of Health. Nine female albino rats (Sprague-Dawley; 250–330 g) were used in the acute, voltage-sensitive dye portion of the study. See the Supplemental Experimental Procedures for details of the surgical preparation. Behavioral studies were conducted using nine female Sprague-Dawley rats (Charles River Laboratories; 7 weeks of age; 250 g at the beginning of the study), which were separate from those in the acute portion of the study. Six animals were trained in the behavioral detection and discrimination tasks, whereas an additional three animals were implanted with an array of recording electrodes in the ventroposterior medial (VPm) nucleus of the thalamus and were subsequently trained in the detection task alone. Animals were housed on a 12 hr reversed light/dark cycle with all experimental sessions occurring during the dark phase.

Vibrissa Stimulation

A multilayered piezoelectric bending actuator (range of motion: 1 mm; bandwidth: 200 Hz; Polytec PI) generated vibrissa deflections. Each of the three experiments described here utilized stimuli with slightly varying parameters. In the anesthetized VSD experiments, vibrissae were deflected in the rostral-caudal plane in a sawtooth waveform of 17 ms in duration ($\tau = 2$ ms). Each trial had 200 ms of prestimulus recording. In nonadapted trials, a single deflection (800–1,500 /s) was delivered to either one of two adjacent vibrissae. In adapted trials, the same probe was preceded by a 1 s, 10 Hz pulsatile adapting stimulus. Stimulation protocols were presented in a random order and repeated 50 times with a minimum of 3.8 s of rest between trials. In the awake/behaving detection and discrimination experiments, whisker deflections were ramp and hold stimuli similar to those used in previous studies (Stüttgen and Schwarz, 2008) and were always delivered in the rostral to caudal direction. The actuator tip followed a quarter sine wave trajectory from rest to its most caudal position, subtending a total of 14 . The amplitude of stimuli remained fixed and the time to the maximum amplitude was varied to control the deflection velocity. After reaching its maximum amplitude, the whisker was held for 1 s, before slowly being returned to rest over 2 s. This slow return phase was designed to be below the animals' perceptual threshold, thus ensuring that the behavioral response was triggered on the rising phase of the stimulus. On half of the trials (see description of behavioral task below), a 3 s, 12 Hz sine wave adapting stimulus subtending ±14 was applied prior to the detection or discrimination stimulus. Velocities in the detection task ranged from 25 /s to 2,500 /s. In the discrimination task, a single deflection velocity of 1,500 /s was used. For experiments with chronically implanted thalamic recording electrodes, the adapting stimulus was replaced with a 3 s, 10 Hz series of 1,500 /s, 10 ms pulsatile stimuli similar to that used in Wang et al. (2010). The ramp-and-hold probe stimulus was replaced with a single 10 ms stimulus with a velocity of 1,500 /s. These brief, pulsatile stimuli provided much better defined events against which to measure the neural response. See the Supplemental Experimental Procedures for further details of the stimulus design.

VSD Imaging and Data Analysis

The VSD imaging techniques have been previously reported (Wang et al., 2012; see Supplemental Experimental Procedures). All analyses of VSD data were conducted in Matlab, and based on the change in the fluorescence relative to the background, or $\Delta F/F_0$. Specifically, the VSD frames were divided by the background image F_0 in a pixel-wise fashion. Additionally, to account for nonstationarities in the imaging data, a baseline frame was subtracted from all frames to ultimately form ΔF. For nonadapted trials and prestimulus frames, the baseline was the average of the first 50 ms of prestimulus frames. For adapted trials, the baseline was the first 50 ms immediately preceding the probe. The resulting frames were divided by the background F_0, to produce our primary measure $\Delta F/F_0$. The prestimulus frames (excluding those used as the baseline) within each trial were time-averaged every four frames.

Ideal Observer Analysis

Detection

The primary region response variable was defined as the decision variable (DV) for this analysis. For each of the three cases, prestimulus noise, nonadapted response, and adapted response, the DVs from all single trials were binned and fit with a Gaussian function to represent the probability mass function. The noise distribution was formed by the decision variables extracted from

all prestimulus frames. We measured detectability using a standard detection theory variable, d′, which quantifies the separability between two distributions, for both the adapted and nonadapted cases relative to the noise. See the Supplemental Experimental Procedures and Figures S2O and S2P for additional measures.

Discrimination

For all single trials given whisker 1 stimulation, both response variables from region 1 ($R_1|W_1$) and region 2 ($R_2|W_1$) were extracted and plotted as a cluster, and the response variables from whisker 2 stimulation were plotted as another cluster. LDA was used to optimally separate the two clusters (Fisher linear discriminant, Matlab). The response variables were then projected onto the axis orthogonal to the LDA line and formed two histograms and each was fitted a Gaussian probability distribution. The projected response variable is defined as the decision variable. The separation of the decision variable distributions, measured as d′, was used as the discriminability measure. A likelihood ratio test was also performed on the extracted variables (Duda et al., 2001). See the Supplemental Experimental Procedures for details.

Behavioral Procedures

Behavior

The behavioral apparatus and training procedures were similar to those previously reported (Ollerenshaw et al., 2012) and were based closely off of those described in Schwarz et al. (2010). Animals were placed in a custom-built body restraint box designed to limit body movement while allowing the animal to maintain a comfortable position. Animals were water restricted 5 days a week with free water on weekends and performed tasks for water reward. See the Supplemental Experimental Procedures for details of the habituation and water restriction techniques.

Detection/Discrimination Task Design

Animals were initially trained in a go/no-go detection task (Figure 3A) similar to that described previously (Stüttgen and Schwarz 2008; Ollerenshaw et al., 2012). Data were collected from four animals in the detection task and the piezoelectric actuator was placed on the C2 whisker for all animals but one, for which the D1 whisker was used. Two animals were moved directly to the discrimination task (see below) without collecting data in the detection task. See the Supplemental Experimental Procedures for details of the detection task design.

After training in the detection task, animals were subsequently trained in a two-whisker go/no-go spatial discrimination task (Figure 4A). Five of the six animals in the study were moved to this task. See the Supplemental Experimental Procedures for details of the discrimination task design.

Behavioral Data Analysis

Data from the detection task were pooled across four animals in order to construct the psychometric curves shown in Figure 3B. Trials were categorized into three possible types: responses without adaptation (nonadapted), responses to stimuli within 0.5–1.5 s from the end of the adapting stimulus (adapted short recovery), and responses to stimuli within 1.5–2.5 s from the end of the adapting stimulus (adapted long recovery). Trials in which the adapting stimulus was present and the animal emitted an anticipatory lick during the no-lick period, thereby creating a delay between the adapting and probe stimulus greater than 2.5 s, were omitted from the analysis. See the Supplemental Experimental Procedures and Figures S3 and S4 for additional details of the behavioral data analysis.

Thalamic Recordings in the Awake Animal

An array of custom-built microwire recording electrodes were affixed to an adjustable microdrive based on the design described in Haiss et al. (2010) and were chronically implanted prior to behavioral training (see Supplemental Experimental Procedures). All data were analyzed using custom scripts written in Matlab (Mathworks). The number of spikes elicited per stimulus was measured in a 30 ms poststimulus window. We utilized the TC40 metric as a measure of timing precision (Pinto et al., 2000), defined as the number of spikes representing 40% of the total, divided by the time required to produce 40% of the total spikes. See Figure S5 for additional measures.

Thalamocortical Modeling

The network architecture was based on a published model by Kyriazi and Simons (1993), with each neuron modeled as a quadratic integrate and fire neuron (Izhikevich, 2007). Each cortical column included 100 thalamic neurons that projected to a downstream cortical population comprised of 700 excitatory neurons and 300 inhibitory neurons (Simons and Woolsey, 1984; Woolsey et al., 1975). Each cortical layer 4 barrel was treated as an independent unit (Goldreich et al., 1999), and there was assumed to be no connectivity between a given thalamic barreloid and an adjacent cortical barrel (Bruno and Sakmann, 2006; Bruno and Simons, 2002; Oberlaender et al., 2012). Each barreloid was modeled as a homogeneous population of excitatory relay cells that synapse onto both excitatory and inhibitory units in layer 4 of the cortex. The excitatory and inhibitory units in the cortex also synapse onto one another, allowing the model to account for feed-forward inhibition (Gabernet et al., 2005). A schematic of the model is shown in Figure 7A. See the Supplemental Experimental Procedures for additional details of the thalamocortical model architecture and simulations.

SUPPLEMENTAL INFORMATION

Supplemental Information includes Supplemental Experimental Procedures and five figures and can be found with this article online at http://dx.doi.org/10.1016/j.neuron.2014.01.025.

AUTHOR CONTRIBUTIONS

D.R.O., H.J.V.Z., D.C.M., Q.W., and G.B.S. conceived and designed the experiments; D.R.O. conducted the behavioral experiments, collected the awake electrophysiological data, and analyzed the corresponding data; H.J.V.Z. conducted the VSD experiments and analyzed the corresponding data; D.C.M. performed the modeling work; and D.R.O., H.J.V.Z., Q.W., and G.B.S. wrote the paper.

ACKNOWLEDGMENTS

We would like to thank Bilal Bari, Elaina Mclean, Spencer Neeley, Christopher Pace, and Emilio Salazar for assistance with behavioral data collection and Clare Gollnick for assistance with histology. We also thank Dominique Pritchett for helpful conversations regarding task design. This work was supported by the National Institutes of Health (grant R01NS48285) and the National Science Foundation CRCNS program (grant IOS-1131948). D.R.O. was supported by a National Institutes of Health Ruth L. Kirschstein national research service award (F31NS074797), and D.C.M. was supported by a National Science Foundation graduate research fellowship.

Accepted: December 31, 2013
Published: March 5, 2014

REFERENCES

Ahissar, E., Sosnik, R., and Haidarliu, S. (2000). Transformation from temporal to rate coding in a somatosensory thalamocortical pathway. Nature *406*, 302–306.

Alonso, J.M., Usrey, W.M., and Reid, R.C. (1996). Precisely correlated firing in cells of the lateral geniculate nucleus. Nature *383*, 815–819.

Barlow, H.B. (1961). Possible principles underlying the transformation of sensory messages. In Sensory Communication, W. Rosenblith, ed. (Cambridge, MA: MIT Press), pp. 271–274.

Brecht, M., Preilowski, B., and Merzenich, M.M. (1997). Functional architecture of the mystacial vibrissae. Behav. Brain Res. *84*, 81–97.

Brumberg, J.C., Pinto, D.J., and Simons, D.J. (1996). Spatial gradients and inhibitory summation in the rat whisker barrel system. J. Neurophysiol. *76*, 130–140.

Bruno, R.M. (2011). Synchrony in sensation. Curr. Opin. Neurobiol. *21*, 701–708.

Bruno, R.M., and Simons, D.J. (2002). Feedforward mechanisms of excitatory and inhibitory cortical receptive fields. J. Neurosci. *22*, 10966–10975.

Bruno, R.M., and Sakmann, B. (2006). Cortex is driven by weak but synchronously active thalamocortical synapses. Science *312*, 1622–1627.

Butts, D.A., Weng, C., Jin, J., Yeh, C.-I., Lesica, N.A., Alonso, J.-M., and Stanley, G.B. (2007). Temporal precision in the neural code and the timescales of natural vision. Nature *449*, 92–95.

Carvell, G.E., and Simons, D.J. (1990). Biometric analyses of vibrissal tactile discrimination in the rat. J. Neurosci. *10*, 2638–2648.

Castro-Alamancos, M.A. (2004). Absence of rapid sensory adaptation in neocortex during information processing states. Neuron *41*, 455–464.

Chung, S., Li, X., and Nelson, S.B. (2002). Short-term depression at thalamocortical synapses contributes to rapid adaptation of cortical sensory responses in vivo. Neuron *34*, 437–446.

Clifford, C.W.G., Webster, M.A., Stanley, G.B., Stocker, A.A., Kohn, A., Sharpee, T.O., and Schwartz, O. (2007). Visual adaptation: neural, psychological and computational aspects. Vision Res. *47*, 3125–3131.

Crick, F. (1984). Function of the thalamic reticular complex: the searchlight hypothesis. Proc. Natl. Acad. Sci. USA *81*, 4586–4590.

Crochet, S., and Petersen, C.C.H. (2006). Correlating whisker behavior with membrane potential in barrel cortex of awake mice. Nat. Neurosci. *9*, 608–610.

Desbordes, G., Jin, J., Weng, C., Lesica, N.A., Stanley, G.B., and Alonso, J.M. (2008). Timing precision in population coding of natural scenes in the early visual system. PLoS Biol. *6*, e324.

Diamond, M.E., and Arabzadeh, E. (2013). Whisker sensory system: from receptor to decision. Prog. Neurobiol. *103*, 28–40.

Duda, R., Hart, P., and Stork, D. (2001). Pattern Classification and Scene Analysis, Second Edition. (New York: Wiley).

Fairhall, A.L., Lewen, G.D., Bialek, W., and de Ruyter Van Steveninck, R.R. (2001). Efficiency and ambiguity in an adaptive neural code. Nature *412*, 787–792.

Fanselow, E.E., and Nicolelis, M.A. (1999). Behavioral modulation of tactile responses in the rat somatosensory system. J. Neurosci. *19*, 7603–7616.

Fanselow, E.E., Sameshima, K., Baccala, L.A., and Nicolelis, M.A. (2001). Thalamic bursting in rats during different awake behavioral states. Proc. Natl. Acad. Sci. USA *98*, 15330–15335.

Ferezou, I., Haiss, F., Gentet, L.J., Aronoff, R., Weber, B., and Petersen, C.C.H. (2007). Spatiotemporal dynamics of cortical sensorimotor integration in behaving mice. Neuron *56*, 907–923.

Gabernet, L., Jadhav, S.P.S., Feldman, D.E.D.E., Carandini, M., and Scanziani, M. (2005). Somatosensory integration controlled by dynamic thalamocortical feed-forward inhibition. Neuron *48*, 315–327.

Gilbert, C.D., and Li, W. (2013). Top-down influences on visual processing. Nat. Rev. Neurosci. *14*, 350–363.

Goble, A.K., and Hollins, M. (1993). Vibrotactile adaptation enhances amplitude discrimination. J. Acoust. Soc. Am. *93*, 418–424.

Goldreich, D., Kyriazi, H.T., and Simons, D.J. (1999). Functional independence of layer IV barrels in rodent somatosensory cortex. J. Neurophysiol. *82*, 1311–1316.

Haiss, F., Butovas, S., and Schwarz, C. (2010). A miniaturized chronic microelectrode drive for awake behaving head restrained mice and rats. J. Neurosci. Methods *187*, 67–72.

Hentschke, H., Haiss, F., and Schwarz, C. (2006). Central signals rapidly switch tactile processing in rat barrel cortex during whisker movements. Cereb. Cortex *16*, 1142–1156.

Higley, M.J., and Contreras, D. (2006). Balanced excitation and inhibition determine spike timing during frequency adaptation. J. Neurosci. *26*, 448–457.

Houweling, A.R., and Brecht, M. (2008). Behavioural report of single neuron stimulation in somatosensory cortex. Nature *451*, 65–68.

Huber, D., Petreanu, L., Ghitani, N., Ranade, S., Hromádka, T., Mainen, Z., and Svoboda, K. (2008). Sparse optical microstimulation in barrel cortex drives learned behaviour in freely moving mice. Nature *451*, 61–64.

Hutson, K.A., and Masterton, R.B. (1986). The sensory contribution of a single vibrissa's cortical barrel. J. Neurophysiol. *56*, 1196–1223.

Izhikevich, E.M. (2007). Dynamical Systems in Neuroscience. (Cambridge, MA: MIT Press).

Khatri, V., Bruno, R.M., and Simons, D.J. (2009). STIMULUS-specific and stimulus-nonspecific firing synchrony and its modulation by sensory adaptation in the whisker-to-barrel pathway. J. Neurophysiol. *101*, 2328–2338.

Kleinfeld, D., and Delaney, K.R. (1996). Distributed representation of vibrissa movement in the upper layers of somatosensory cortex revealed with voltage-sensitive dyes. J. Comp. Neurol. *375*, 89–108.

Kohn, A., and Whitsel, B.L. (2002). Sensory cortical dynamics. Behav. Brain Res. *135*, 119–126.

Kyriazi, H.T., and Simons, D.J. (1993). Thalamocortical response transformations in simulated whisker barrels. J. Neurosci. *13*, 1601–1615.

LaMotte, R.H., and Mountcastle, V.B. (1979). Disorders in somesthesis following lesions of parietal lobe. J. Neurophysiol. *42*, 400–419.

Lee, C.J., and Whitsel, B.L. (1992). Mechanisms underlying somatosensory cortical dynamics: I. In vivo studies. Cereb. Cortex *2*, 81–106.

Leiser, S.C., and Moxon, K.A. (2007). Responses of trigeminal ganglion neurons during natural whisking behaviors in the awake rat. Neuron *53*, 117–133.

Lesica, N.A., and Stanley, G.B. (2004). Encoding of natural scene movies by tonic and burst spikes in the lateral geniculate nucleus. J. Neurosci. *24*, 10731–10740.

Lesica, N.A., Weng, C., Jin, J., Yeh, C.-I., Alonso, J.-M., and Stanley, G.B. (2006). Dynamic encoding of natural luminance sequences by LGN bursts. PLoS Biol. *4*, e209.

Macmillan, N.A., and Creelman, C.D. (2005). Detection Theory: A User's Guide, Second Edition. (Mahwah, NJ: Lawrence Erlbaum Associates).

Maravall, M., Petersen, R.S., Fairhall, A.L., Arabzadeh, E., and Diamond, M.E. (2007). Shifts in coding properties and maintenance of information transmission during adaptation in barrel cortex. PLoS Biol. *5*, e19.

Moore, C.I. (2004). Frequency-dependent processing in the vibrissa sensory system. J. Neurophysiol. *91*, 2390–2399.

Moore, C.I., Nelson, S.B., and Sur, M. (1999). Dynamics of neuronal processing in rat somatosensory cortex. Trends Neurosci. *22*, 513–520.

Mountcastle, V.B., and Darian-Smith, I. (1968). Neural mechanisms in somesthesia. In Medical Physiology, *Volume II*, V. Mountcastle, ed. (St. Louis: CV Mosby), pp. 1372–1423.

O'Connor, D.H., Clack, N.G., Huber, D., Komiyama, T., Myers, E.W., and Svoboda, K. (2010). Vibrissa-based object localization in head-fixed mice. J. Neurosci. *30*, 1947–1967.

Oberlaender, M., Ramirez, A., and Bruno, R.M. (2012). Sensory experience restructures thalamocortical axons during adulthood. Neuron *74*, 648–655.

Ollerenshaw, D.R., Bari, B.A., Millard, D.C., Orr, L.E., Wang, Q., and Stanley, G.B. (2012). Detection of tactile inputs in the rat vibrissa pathway. J. Neurophysiol. *108*, 479–490.

Petersen, C.C.H., Grinvald, A., and Sakmann, B. (2003). Spatiotemporal dynamics of sensory responses in layer 2/3 of rat barrel cortex measured in vivo by voltage-sensitive dye imaging combined with whole-cell voltage recordings and neuron reconstructions. J. Neurosci. *23*, 1298–1309.

Pinto, D.J., Brumberg, J.C., and Simons, D.J. (2000). Circuit dynamics and coding strategies in rodent somatosensory cortex. J. Neurophysiol. *83*, 1158–1166.

Pouget, A., Deneve, S., Ducom, J.C., and Latham, P.E. (1999). Narrow versus wide tuning curves: What's best for a population code? Neural Comput. *11*, 85–90.

Poulet, J.F.A., Fernandez, L.M.J., Crochet, S., and Petersen, C.C.H. (2012). Thalamic control of cortical states. Nat. Neurosci. *15*, 370–372.

Romo, R., Hernández, A., Zainos, A., Brody, C.D., and Lemus, L. (2000). Sensing without touching: psychophysical performance based on cortical microstimulation. Neuron *26*, 273–278.

Roy, S.A., and Alloway, K.D. (2001). Coincidence detection or temporal integration? What the neurons in somatosensory cortex are doing. J. Neurosci. *21*, 2462–2473.

Schwarz, C., Hentschke, H., Butovas, S., Haiss, F., Stüttgen, M.C., Gerdjikov, T.V., Bergner, C.G., and Waiblinger, C. (2010). The head-fixed behaving rat—procedures and pitfalls. Somatosens. Mot. Res. *27*, 131–148.

Sclar, G., Lennie, P., and DePriest, D.D. (1989). Contrast adaptation in striate cortex of macaque. Vision Res. *29*, 747–755.

Sherman, S.M. (2001). Tonic and burst firing: dual modes of thalamocortical relay. Trends Neurosci. *24*, 122–126.

Sheth, B.R., Moore, C.I., and Sur, M. (1998). Temporal modulation of spatial borders in rat barrel cortex. J. Neurophysiol. *79*, 464–470.

Simons, D.J., and Woolsey, T.A. (1984). Morphology of Golgi-Cox-impregnated barrel neurons in rat SmI cortex. J. Comp. Neurol. *230*, 119–132.

Simons, D.J., and Carvell, G.E. (1989). Thalamocortical response transformation in the rat vibrissa/barrel system. J. Neurophysiol. *61*, 311–330.

Simons, D.J., Carvell, G.E., Hershey, A.E., and Bryant, D.P. (1992). Responses of barrel cortex neurons in awake rats and effects of urethane anesthesia. Exp. Brain Res. *91*, 259–272.

Simons, S.B., Tannan, V., Chiu, J., Favorov, O.V., Whitsel, B.L., and Tommerdahl, M. (2005). Amplitude-dependency of response of SI cortex to flutter stimulation. BMC Neurosci. *6*, 43.

Stanley, G.B. (2013). Reading and writing the neural code. Nat. Neurosci. *16*, 259–263.

Stanley, G.B., Jin, J., Wang, Y., Desbordes, G., Wang, Q., Black, M.J., and Alonso, J.-M. (2012). Visual orientation and directional selectivity through thalamic synchrony. J. Neurosci. *32*, 9073–9088.

Stüttgen, M.C., and Schwarz, C. (2008). Psychophysical and neurometric detection performance under stimulus uncertainty. Nat. Neurosci. *11*, 1091–1099.

Tannan, V., Whitsel, B.L., and Tommerdahl, M.A. (2006). Vibrotactile adaptation enhances spatial localization. Brain Res. *1102*, 109–116.

Temereanca, S., Brown, E.N., and Simons, D.J. (2008). Rapid changes in thalamic firing synchrony during repetitive whisker stimulation. J. Neurosci. *28*, 11153–11164.

Tommerdahl, M., Favorov, O., and Whitsel, B.L. (2002). Optical imaging of intrinsic signals in somatosensory cortex. Behav. Brain Res. *135*, 83–91.

Usrey, W.M., Alonso, J.M., and Reid, R.C. (2000). Synaptic interactions between thalamic inputs to simple cells in cat visual cortex. J. Neurosci. *20*, 5461–5467.

Vierck, C.J., Jr., and Jones, M.B. (1970). Influences of low and high frequency oscillation upon spatio-tactile resolution. Physiol. Behav. *5*, 1431–1435.

von Békésy, G. (1957). Neural volleys and the similarity between some sensations produced by tones and by skin vibrations. J. Acoust. Soc. Am. *29*, 1059–1069.

Wang, Q., Webber, R.M., and Stanley, G.B. (2010). Thalamic synchrony and the adaptive gating of information flow to cortex. Nat. Neurosci. *13*, 1534–1541.

Wang, Q., Millard, D.C., Zheng, H.J.V., and Stanley, G.B. (2012). Voltage-sensitive dye imaging reveals improved topographic activation of cortex in response to manipulation of thalamic microstimulation parameters. J. Neural Eng. *9*, 026008.

Woolsey, T.A., Dierker, M.L., and Wann, D.F. (1975). Mouse SmI cortex: qualitative and quantitative classification of golgi-impregnated barrel neurons. Proc. Natl. Acad. Sci. USA *72*, 2165–2169.